RSC Advances

PAPER

View Article Online
View Journal | View Issue

Cite this: *RSC Adv.*, 2022, **12**, 15284

Polymerization kinetics of bicyclic olefins and mechanism with symmetrical ansa-metallocene catalysts associated with active center count: relationship between their activities and structure and activation path†

Amjad Ali, [ai] Ahmad Naveed,[a] Khurram Shehzad, [*bcd] Tariq Aziz, [e] Tahir Rasheed,[f] Jamile Mohammadi Moradian,[g] Mobashar Hassan,[a] Abdul Rahman,[bh] Fan Zhiqiang [i] and Li Guo [*a]

Copolymerization of ethylene (E) with 5-vinyl-2-norbornene (VNB) catalyzed by ansa-metallocenes allows the precise control of essential polymeric properties such as comonomer incorporation, molecular weight (M_w), and polydispersity ($Đ$). Significant efforts have been devoted to synthesizing and developing novel catalysts, cocatalysts, and activators, although the fundamental elements of catalytic processes remain unclear. For example, it is questionable how polymeric catalysts are divided across dormant and active sites and how this distribution affects the order of monomers for the propagation rate, which widely vary in the literature. Furthermore, although the empirical correlation between the monomers and average M_w has been established in many systems, the fundamental processes of chain termination remain unknown. Furthermore, the involvement of ion-pairing in metallocene-catalyzed polymerization and the termination mechanisms are also contentious issues. In this study, we describe the use of a quenched-labeling technique based on acyl chloride to selectively quench the zirconium metal–polymeric bond, which can be used to study the kinetics, active site [Zr][C*] counting, copolymer microstructure, and molecular weight distribution (MWD) to determine the rate laws for chain initiation, chain propagation rate (R_p), propagation rate constant (k_p) and chain termination. In addition, we also predict previously unknown chemical characteristics of E/bicyclic copolymerization processes, where either a *cis*-endocyclic double bond with steric properties or a vinyl exocyclic double bond affects the activity, *i.e.*, [Zr]/[*C], (R_p) and (k_p). All these properties require the implementation of a particular kinetic mechanism that assumes the low activity of the building copolymer chains incorporating a single ethylene/VNB unit, *i.e.*, the $Cp_2Zr–C_2H_5$ group, in the ethylene addition process in the $Cp_2Zr–C$ bond. Due to β-agostic stabilization, the $Cp_2Zr–C_2H_5$ group exhibits a distinct feature. These effects were confirmed experimentally, such as the E/VNB co-polymer activity and VNB mol%, propagation rate decrease in the polymerization time (t_p) of 120 s to 1800 s, crystalline properties, and significant increase in molecular weight. The active center [Zr]/[*C] fraction considerably increased in the initial (t_p) 840 s, and subsequently tended to the steady stage of 33%, which is lower than previously reported E homo- and E/P copolymerization. The lower [C*]/[Zr] in both the early and stable stages, decrease in VNB mol%, and R_p with t_p can be associated with the more significant fraction of $Cp_2Zr–CH_2CH_3$-type dormant site by

Received 25th February 2022
Accepted 2nd April 2022

DOI: 10.1039/d2ra01264b

rsc.li/rsc-advances

[a]*Research School of Polymeric Materials, School of Materials Science & Engineering, Jiangsu University, Zhenjiang, 212013, P. R. China. E-mail: liguo@ujs.edu.cn*

[b]*School of Micro-Nano Electronics, Hangzhou Global Scientific and Technological Innovation Center (HIC), Zhejiang University, Xiaoshan 311200, China. E-mail: khurrams@zju.edu.cn*

[c]*State Key Laboratory of Silicon Materials, Zhejiang University, Hangzhou 310027, China*

[d]*ZJU-UIUC Joint Institute, Zhejiang University, Jiaxing 314400, China*

[e]*Westlake University, School of Engineering Yunqi Campus, Hangzhou, Zhejiang 310024, PR China*

[f]*Interdisciplinary Research Center for Advanced Materials, King Fahd University of Petroleum and Minerals (KFUPM), Dhahran 31261, Saudi Arabia*

[g]*Biofuels Institute, School of Envinoment, Jiangsu University, Zhenjiang, 212013, P. R. China*

[h]*Stoddart Institute of Molecular Science, Department of Chemistry, Zhejiang University, Hangzhou 310027, China*

[i]*MOE Key Laboratory of Macromolecular Synthesis and Functionalization, Department of Polymer Science and Engineering, Zhejiang University, Hangzhou, 310027, P. R. China*

† Electronic supplementary information (ESI) available. See https://doi.org/10.1039/d2ra01264b

the β-agostic hydrogen interaction with the Cp_2Zr metal. The t_p *versus* R_pE, R_pVNB, k_pE, k_pVNB, and [Zr]/[C*] count could be fitted to a model that invokes deactivation of the growing polymer chains. In the case of the thermal behavior of the copolymers (melting temperature (T_m) and crystalline temperature (ΔH_m)), T_m varied from 101 °C to 121 °C, while ΔH_m varied from 9 to 16 (J g^{-1}).

Introduction

Homogeneous catalysts can be used to precisely regulate the properties of polymer such as their microstructure, molecular weight (M_w), and dispersity index ($Đ$).[1–6] The modern homogeneous metallocenes can covert simple alkenes into polymers with the regio-stereospecificity and rate accelerations surpassing that of enzymatic catalysts.[7–9] Catalysis is purely a kinetic phenomenon.[10–13] Given the previous impact of metallocene catalysts on polyolefin research and manufacturing, it was surprising that there are no well-defined rate laws for the fundamental steps of polymerization such as initiation (k_i) by the addition of monomers to the metal–polymeric bond, chain propagation (k_p), re-initiation from a metal–hydrogen bond (M–H) bond and chain termination for a logical and practical metallocene-catalyzed polymerization reaction with applicable propagation rate (R_p).[14–18] The absence of well-defined rate laws is partially attributed to the problems posed by metallocene catalysts with high catalytic activity and great sensitivity to contaminants.[19–21] In addition, it is difficult to identify the percentage of metallocenes dynamically constructing a polymer in any instant, such as the active site count. Thus, it is challenging to accept empirical rate laws with molecular pathways without information on the concentration and speciation of the catalytically dynamic species.[22,23] In the literature, many theoretical investigations have been reported on monomer insertion, the role of cocatalyst, activity, and polymerization mechanism of metallocene systems. In this contribution, a methylalumoxane (MAO) cocatalyst, which includes various activating species, complicates the study given that it could further speciate the active catalytic sites.[24,25] As shown in Scheme S1,† the critical features of the model are as follows: (1) ion-pair solvent separation occurs before alkene insertion; simple bimolecular mechanisms accomplish (2) initiation and propagation; and (3) β-hydride elimination is the predominant chain termination step. However, it is difficult to explain many facts with this straightforward explanation.[26–28] Thus, this basic model cannot explain a large amount of data.

The commercial production of EPE EPDM olefins by polymerization exceeds 100 million tons per year. Some kinetic polymerization investigations assume that 100% of the polymeric catalyst added to the system is active during the reactions.[29,30] However, numerous comprehensive kinetic investigations showed wide variations in the active sites amongst the different catalysts used in olefin polymerization. In addition, identical polymeric catalysts can have variable active site concentrations, depending on the reaction parameters, for example, monomer pressure, temperature, solubility of monomers, additives, and activators. In fact, in homogenous metallocenes, their active center concentration is less than 5% and even 1%. Therefore, it is essential to determine why some metallocenes have higher active site counts and others do not. This is critical for understanding the chemistry of catalysts and the polymerization procedure more generally. Also, it is challenging but essential to identify the origin of 100% polymerization catalyst activity, which can lead to significant improvements in catalyst productivity due to the optimization of the reaction conditions or catalyst design.[6,31,32]

Generally, polymerization reactions are seriously impacted by either the low efficiency of the selected comonomers or the excessive amount of comonomers chosen, despite being achievable with some late transition metal-based catalysts and cocatalysts.[18,33,34] Determining the source of 100% catalyst activity may lead to a considerable increase in catalytic efficiency based on changes in the catalyst design or reaction parameters.[35–37] Nonetheless, no kinetic and mechanistic study of the [*rac*-$Me_2Et(Ind)_2ZrCl_2$]/[$(Ph_3C)B(C_6F_5)_4$]-catalyzed copolymerization processes of ethylene with cyclic olefins (E/VNB) with quench flow observation has been published to date. The study of the kinetics of E/VNB copolymerization with the involvement of [*rac*-$Me_2Et(Ind)_2ZrCl_2$]/[$(Ph_3C)B(C_6F_5)_4$]/TIBA using the TPCC technique perfectly demonstrates that the metal–polymeric species provides an efficient method for the real-time measurement of the commoner consumption and catalyst species diversity as a function of time. TPCC works by selectively quenching the metal–polymer bonds through acyl chloride, which has been proven in studies using nickel–diimine, metallocene/MMAO, metallocene/TEA, metallocene/TIBA, and Ziegler–Natta heterogeneous catalyst polymerization reactions.[19,35,38–40] Furthermore, all the obtained E/VNB were characterized *via* ^{1}HNMR, GPC and DSC.

Overall procedures and materials

Standard glovebox and Schlenk-line procedures were used for all reactions under an Ar or pure N_2 environment. A gas purification column and molecular sieves were employed to purify ethylene. Cyclic comonomer 5-vinyl-2-norbornene (VNB) was manufactured by Aldrich, which was dehydrated by stirring with CaH_2 overnight. The catalyst (*rac*-$Et(Ind)_2ZrCl_2$) was purchased from Sigma-Aldrich and its solution prepared in toluene. Triisobutylaluminum (TIBA) was purchased from Albemarle Co. and diluted in heptane. Borate $(Ph_3C)B(C_6F_5)_4$ was synthesized according to the literature and dissolved in toluene for the reaction.[40,41] TPCC with 98% purity was bought from J&K Scientific and prepared as a 2 M solution in dry heptane.

Polymerization

All the E/VNB copolymers reactions were carried out in a 100 mL round-bottom Schlenk flask to ensure uniform polymerization. Thirty minutes before starting the polymerization process, the reactor was heated to 90–100 °C under vacuum before being

backfilled with N_2 gas. An appropriate amount of toluene was added to the Schlenk flask reactor, and then saturated with E. After introducing VNB in the reactor, 2 M TIBA was added, operated for 5 min, and then the appropriate amount of zirconocene catalyst and borate in toluene solutions was added. TPPC (TPCC/Al = 2) was added after the polymerization reaction was complete. In addition, to decompose the borate, metallocene, TPCC, and TIBA, 2% HCl was used. The obtained copolymers were washed several time with 95% ethanol, and subsequently dried under vacuum.[40–42]

Characterizations

A YHTS-2000 fluorescence sulfur detector was employed to measure the sulfur (S) content in each copolymer sample. Using the average of three sulfur (S) content measurements for each sample, the percentage of sulfur was calculated.

The S content in the blank E/VNB copolymers prepared under similar conditions, without TPPC quenching was 0. Then, it was compared with the quench-labelled E/VNB copolymer, which contained an S content ranging from 5 to 35 ppm. The mechanistic model presented in Scheme S2† briefly explains the TPCC quenching phenomena. How the combination of E and VNB produces non-active sites, how the VNB exocyclic double bonds interact with the Zr metal and interact with the catalyst ligand, and how VNB activates the inactive sites is discussed in the later sections herein.

^{1}HNMR

The content of the commoner (VNB) was calculated *via* ^{1}HNMR spectroscopy. ^{1}HNMR spectra were recorded using a Varian Mercury Plus 300 spectrometer. The measurements were performed in *o*-dichlorobenzene-d_4 at 120 °C. Hexamethyldisiloxane was used as the internal reference. Previously reported literature was employed to conform to the E/VNB ^{1}HNMR peak assignment.[41] The ^{1}HNMR spectrum of the E/VNB copolymers used for the kinetic and mechanistic study is presented in the ESI, Fig. S4.† The peaks at 4.5 and 5.4 ppm confirmed the insertion of the endocyclic π bond in the polymer backbone.[43–45]

The thermal properties of the E/VNB copolymers were performed using differential scanning calorimetry (DSC) analysis. The TA Q200 (DSC) instrument was calibrated with water and indium. An appropriate amount of polymer sample was sealed in an aluminum pan. To eliminate the thermal history of the sealed sample, it was firstly heated to 150 °C for 5 min. Secondly, it was cooled at a rate of 10 °C min^{-1} to 20 °C. Finally, it was gradually heated to 180 °C at a rate of 10 °C min^{-1} to produce the melting curve.[46,47]

The polydispersity and molecular weight of E/VNB were calculated *via* high-temperature PL 220 gel permeation chromatography (GPC). The eluent 1,2,4-trichlorobenzene was used in the PL-gel 10 m MIXED-B column with a flow rate of 1.0 mL min^{-1} at 150 °C. It was envisioned that thin polystyrene standards would be used for universal calibration.

Results and discussion

E/VNB copolymerization with zirconocenes/borate/TIBA was firstly studied. For the kinetic and mechanistic studies of these catalyst systems, a series of E/VNB copolymerization tests was performed. The subsequent protocol was followed to maintain the performance of the catalyst, where after injecting VNB, a suitable amount of TIBA was added, which reacted with VNB and the solvent impurities. Our group reported the synthesis of ethylene–propylene co- and E/P/diene terpolymers with a symmetrical metallocene catalyst activated by MMAO and TIBA/borate cocatalyst system.[17,36,39] We observed that the addition of diene decreased the polymerization activity.[19,20,41,48] Herein, we performed our experiments with a stoichiometric amount of VNB 0.06 mol L^{-1}. The time-dependent variation of R_pE and R_pVNB was determined from the differentiation of the curve of copolymer yield *versus* polymerization time (t_p). The sulfur (S) content of the copolymers was calculated in the purified samples to measure [C*]/[Zr] according to the equation [S] = [C*], as shown in ESI Tables S1 and S2.† The propagation rate constants k_pE and k_pVNB were calculated according to the equation $R_p = k_p[C^*][M]$, which was developed for homogenous metallocenes, α-diamine nickel complexes, and heterogeneous Ziegler–Natta catalysts.[38–40] The results of the E/VNB copolymerization, including activity, M_w, MWD, time-dependent [C*]/[Zr] fraction, R_pE, k_pVNB, k_pE, k_pVNB, and thermal properties are summarized in Tables 1 and 2.

According to the literature, the amount of linear conjugated, non-conjugated, and cyclic dienes increases in the reaction system, and as predicted, the activities of metallocene, Ziegler–

Table 1 Ethylene–VNB copolymerization catalyzed by (*rec*-Et(Ind)$_2$ZrCl$_2$)/(Ph$_3$C)B(C$_6$F$_5$)$_4$[a]

RUN	Time (s)	VNB in polymer[b]	Activity (10^7 g_{poly} Mt^{-1} h^{-1})	M_w[c] (g mol^{-1})	PD[c]	T_m[d] (°C)	ΔH_m[d] (J g^{-1})
1.1	120	10.92	0.36	14 100	2.08	122.14	7.78
1.2	240	9.33	0.20	15 100	2.25	120.43	9.77
1.3	360	8.46	0.15	16 000	2.45	120.44	9.48
1.4	480	8.05	0.13	17 800	2.69	120.12	15.01
1.5	840	7.85	0.12	21 000	3.20	120.28	14.92
1.6	1200	7.22	0.11	25 500	3.15	120.62	3.66
1.7	1500	7.09	0.10	27 300	3.27	120.49	12.76
1.8	1800	5.73	0.09	29 300	3.70	121.46	6.41

[a] Reaction conditions: toluene = 50 mL, E = 0.1 MPa, VNB = 0.06 mol L^{-1}, TIBA 1000 μmol, borate = 2.50 μmol, catalyst = 1.25 μmol and TPCC = 2000 μmol. [b] Determined by high-temperature ^{1}HNMR. [c] Determined by high-temperature GPC. [d] Determined by DSC.

Table 2 Ethylene–VNB copolymerization with kinetic data[a]

RUN	Time (s)	VNB in polymer	*C[b] (%)	R_pVNB[c] (mol_{VNB} mol_{cat}^{-1} s^{-1})	R_pE[c] (mol_E mol_{cat}^{-1} s^{-1})	k_pE[d] (L mol^{-1} s^{-1})	k_pVNB[d] (L mol^{-1} s^{-1})
1.1	120	10.92	5.71	0.7	10.23	4266	233
1.2	240	9.33	7.55	0.67	9.87	3113	173
1.3	360	8.46	10.1	0.58	9.52	2244	116
1.4	480	8.05	14.08	0.52	9.18	1552	78.9
1.5	840	7.85	19.68	0.36	8.25	998	42.04
1.6	1200	7.22	26.17	0.25	7.41	674	23.395
1.7	1500	7.09	29.93	0.18	6.77	539	15.727
1.8	1800	5.73	31.67	0.14	6.19	465	11.5397

[a] Reaction conditions: toluene = 50 mL, E = 0.1 MPa, VNB = 0.06 mol L^{-1}, TIBA 1000 μmol, borate = 2.50 μmol, catalyst = 1.25 μmol and TPCC = 2000 μmol. [b] *C determined through the sulfur analyzer (see ESI). [c] R_pVNB and R_pE in units of $mmol_{poly}$ mol_{Mt}^{-1} s^{-1}. [d] Propagation constant of VNB and E.

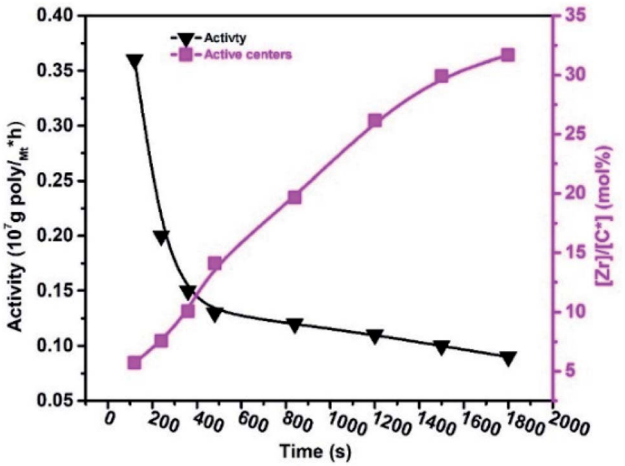

Fig. 1 Change in the active centre [Zr]/[C*] fraction and catalytic activity with polymerization time (t_p) during E/VNB copolymerization.

Natta, and α-diamine nickel polymeric catalysts decrease.[20,33,39] For example, VNB was used as a commoner, similar to ENB used in EPDM manufacturing, but the response of ENB against the metallocene is much more complicated than VNB.[20,48] In E/VNB copolymerization, the activity decreased in the time of 120–1800 s, and [Zr]/[*C] considerably increased, and consequently tended to the stable level of 31.67%. This is similar to polypropylene (PP) but lower than E homo, E/P and E/ENB copolymerization.[17,39,49] The addition of 0.06 mol L^{-1} VNB resulted in the maximum activity of 0.36×10^7 g mol_{Mt}^{-1} h^{-1} at 120 s, as shown in Fig. 1. However, when the reaction time increased, the activity declined until it reached 0.09×10^7 g mol_{Mt}^{-1} h^{-1}. The obtained copolymers containing higher than 5 mol% VNB were soluble in 1,2,4-trichlorobenzene at temperatures greater than 100 °C. Swaminathan Sivaram *et al.* demonstrated that increasing the mol% of dienes in the feed reduces the intrinsic viscosity of the polymer and catalytic activity.[50]

We observed that the effect of VNB on metallocene activity was lower in the initial stage of the reaction than the later stage. It is recommended that metallocene/borate presented a high E/VNB copolymerization rate at 120 s, which can be used to confirm the quick initiation of the active catalytic sites. The plot of R_pE and k_pVNB with t_p is shown in Fig. S3.†

In contrast, the rapid increase in active centres in the initial polymerization level also defined the immediate commencement of active sites located on the surface of the metallocene catalyst molecules. These active sites are the molecules that are accessible to incoming monomers and activators and can be activated during the pre-contact process. Guo *et al.* well-defined in their study the increase in the amount of the deactivated or dormant sites in the metallocene/MAO system by the interaction of the metallocene catalyst with TMA, and they recommended the incomplete activation of the catalyst.[36] In our previous study, we explained that chain transfer with alkylaluminum led to polyethene (PE) chains ending with saturation.[17,19] During the E/VNB copolymerization, a significant change in the solvent reaction viscosity was observed, and the growing polymer fibres entangled on the reaction stirrer were noted. The developing catalytic active sites are compressed in the precipitated copolymers through this phase, inhibiting the incoming monomers from diffusing into the active sites, which subsequently reduces the polymerization rate.

The M_w of the E/VNB copolymerization decreased in the initial polymerization time and slightly increased with an increase in the reaction time. When correlated with the M_w of PE, E/P, and E/ENB copolymers produced with *rac*-Et(Ind)$_2$-ZrCl$_2$/MAO, *rac*-Et(Ind)$_2$ZrCl$_2$/MMAO, and *rac*-Et(Ind)$_2$ZrCl$_2$/TIBA, that of the E/P copolymers is comparable. However, PE and E/ENB were produced with a higher molecular weight. This suggests that the chain transfer of the active sites with the TIBA cocatalyst in the E/VNB copolymers is much faster than that in the PE and E/VNB systems. The MWD of the E/VNB copolymers was broader and became even broader as the reaction time reached 1800 s, which was significantly greater than 2. According to the literature, a theoretical polydispersity index ($Đ$) more than 2 of a true single-site metallocene suggests the presence of numerous active sites in the system (see Fig. S1†).

^{1}HNMR is one of the main methodologies to elucidate the microstructure of polymers and calculate the co-monomer content. It can be observed that the ^{1}HNMR spectra of all the E/VNB copolymer samples demonstrated identical peaks, which are consistent with that reported by Randall *et al.*[51] VNB exhibits two different double bonds, with the peaks for the distinct exocyclic vinyl pattern between 4.5 and 5.9 ppm in the copolymer backbone, and the absence of a strong triplet peak at

6.1 ppm for the endocyclic π bonds, as shown in Fig. S5.† The exocyclic π bonds are nearly nonreactive with the Z–N catalyst. VNB, being a commoner with bulky alkyl groups, has more considerable ring strain, leaving the exocyclic bond unreacted. The exocyclic unreacted bonds were also used to quantify the mol% of VNB comonomers. The mol% of VNB is more significant in the initial reaction time than later. The [Zr]/[C*] rapidly increased initially, presenting evidence of the quick activation of the active sites at the start of the reaction, which was dormant for ethylene polymerizations.

It is well known that 5–10% of dienes are the essential requirement of applicable industrial elastomers. The properties of E/VNB copolymers depend on the VNB content, and the resulting polymers have a melting temperature (T_m) of 100–120 °C or are amorphous. The effect of time and VNB mol% on the thermal properties of the E/VNB copolymers is illustrated in Table 1. Commonly, the cyclic olefins NB, ENB, and VNB are bulkier structures than E or P, and cyclic olefins constrain the rotational movement of the polymers, resulting in a direct effect on their thermal properties such as crystalline (ΔH_m) and melting temperature (T_m).

The E/VNB copolymer ΔH_m temperature varies from 9 to 16 (J g^{-1}) and T_m ranges from 100 °C to 120 °C. In addition, these results are strongly based on endocyclic π and exocyclic π insertion and the VNB composition. According to the analysis of the HNMR spectra, that endocyclic π-inserted VNB and exocyclic π composition is more than 5 mol%. E/VNB copolymers with VNB-rich segments were obtained in the earlier stage if the reaction melted at a lower temperature, and later due to the higher solubility of E, the incorporation of VNB decreased and it melted at a higher temperature. Interestingly, we discovered that the crystallinity of the E/VNB copolymer was lower and the initial polymerization rates (R_pE and R_pVNB) were higher due to the more significant insertion of VNB into the growing polymer chain. As the reaction time increased, the mol% of VNB and R_pE and R_pVNB in the E/VNB copolymers decreased. This is because the chain termination response in E/VNB is more rapid in the latter stage than the early stage.

The results of the E/VNB copolymerization, including time-dependent [C*]/[Zr], are summarized in Table 2, together with the kinetic data including R_pVNB, R_pE, k_pVNB, and k_pE. As shown in Fig. 2 and 3, all the kinetic properties studied, such as R_pVNB, R_pE, k_pVNB, and k_pE with t_p, showed a moderate decrease.

In contrast, the active sites continuously increased with time t_p. The E/VNB copolymers had a lower [C*]/[Zr] fraction (3–8% at 240 s), but later, the system reached 33.7% in 1800 s. In previous studies, the same catalyst system-catalyzed E/ENB copolymers showed a much greater initial [C*]/[Zr] fraction (16–30% at 240 s) and relativity quicker increase in the active centers up to stable stage. During the E homo polymerization after 1800 s, the reaction time [C*]/[Zr] fraction reached 73%, which is higher

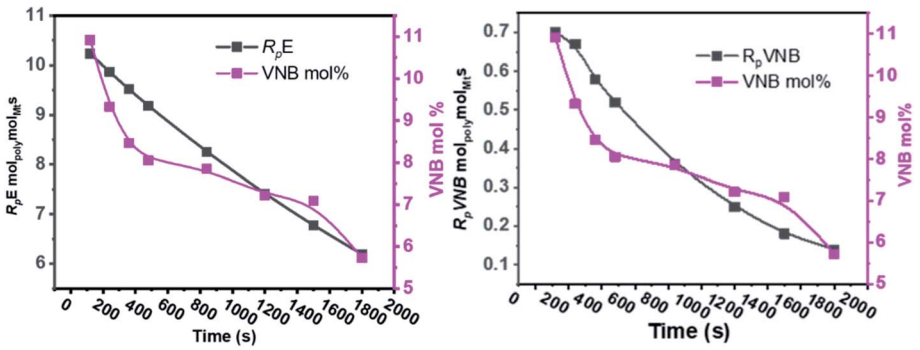

Fig. 2 As the polymerization time progressed, the amount of VNB in mol% and the ratios of R_pE and R_pVNB decreased.

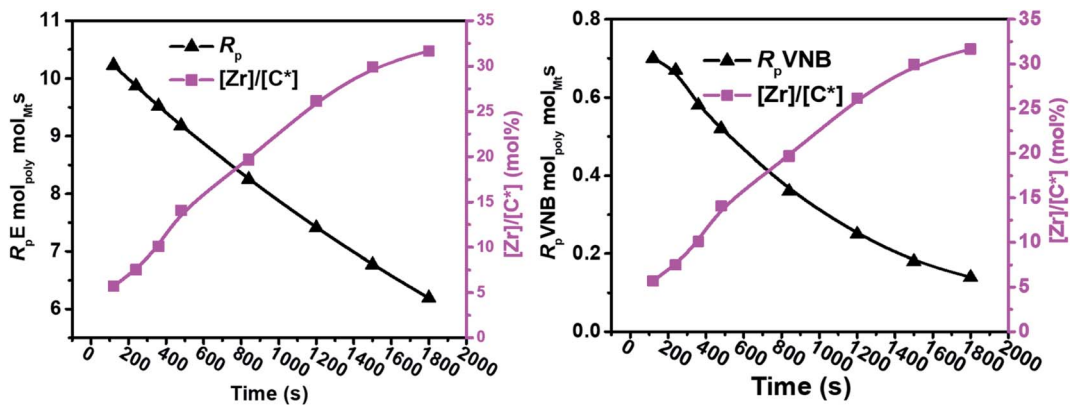

Fig. 3 Fluctuation in the active center fractions R_pE and R_pVNB in the E/VNB copolymers as a function of polymerization time.

than that of this system. Thus, this means that ethylene copolymerized with ENB and VNB has different characteristics. Alternatively, k_pE, k_pVNB, and k_pVNB are much lower than k_pE, which suggests that the minor diffusion barriers in the early stages are close to the actual propagation rate constant. Similarly, at 120 s, the k_pE and k_pVNB values were 4466 and 233 L mol^{-1} s^{-1}, respectively, which are lower than that of the PE and E/ENB polymers, indicating that the diffusion barriers in E/VNB are higher than that in the PE and E/ENB systems.

When considering the continuous decrease in k_pE and k_pVNB with the polymerization time, this may be due to the drop in the local-monomer concentration around the active site as a result of the diffusion barrier, given that the rate of monomer diffusion from the bulk of solution to the position of active sites quickly decreased once the first set of polymerization chains was formed and aggregated in and around the active sites of the catalyst.

As shown in Fig. 4, in the early 500 s, an increase in the [Zr]/[C*] percentage by more than threefold was observed. The potential reactivity variation across the active sites triggered at various reaction phases may also have caused a significant variation in the k_pE and k_pVNB values. This is because the active catalytic sites in the time range of 120–480 s are 30% more active than the active catalytic sites in the later time range. The former account for 40% of the total [Zr]/[C*], and the average k_pE and k_pVNB values at the polymerization time of 1000 s were only 50% of that at the polymerization time of 480 s. Thus, it is reasonable to assume that there is no diffusion barrier in the system. In contrast, as reaction time increased, both k_pE and k_pVNB and the mol% of VNB decreased, as shown in Fig. 5.

The formerly investigated initial k_pPE of polyethene and E/ENB copolymerization k_pE values differed, whereas the k_pPE of polyethene and k_pE of the E/VNB copolymer were the same at 120 s (4110, 9115, and 4266, respectively). This is because the [C*]/[Zr] fraction of E/VNB copolymerization at the initial level is the same with polyethene but lower than that of the E/ENB copolymers, indicating that PE and E/VNB have the same type of active centers, whereas that if E/ENB is different. The active centers in the polyethylene and E/VNB copolymerization that produce E/VNB copolymers may be made up of contact ion pairs with lower k_pPE and k_pE values. In contrast, the active center in the E/ENB copolymers could be made up of loosely associated ion pairs with higher k_pE values. Thus, to make the comparisons among the k_p of PE, E/ENB, and E/VNB polymerization more understandable, the curves of polymerization time *vs.* k_p are illustrated in Fig. 6 and 7.

The initial values of k_pE and k_pVNB of E/VNB are similar with that of E/P but lower than that of the E/ENB polymers because E/

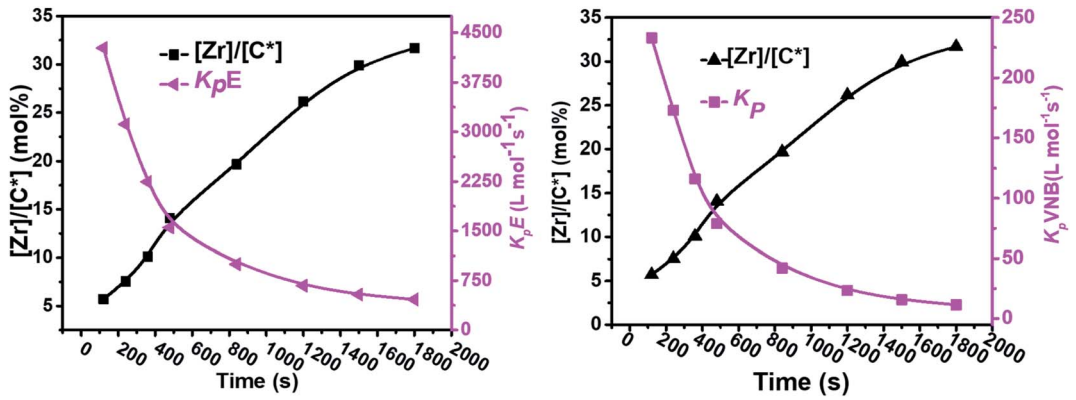

Fig. 4 Variation in the propagation rate constants k_pE and k_pVNB and active center fraction in the E/VNB copolymers with polymerization time.

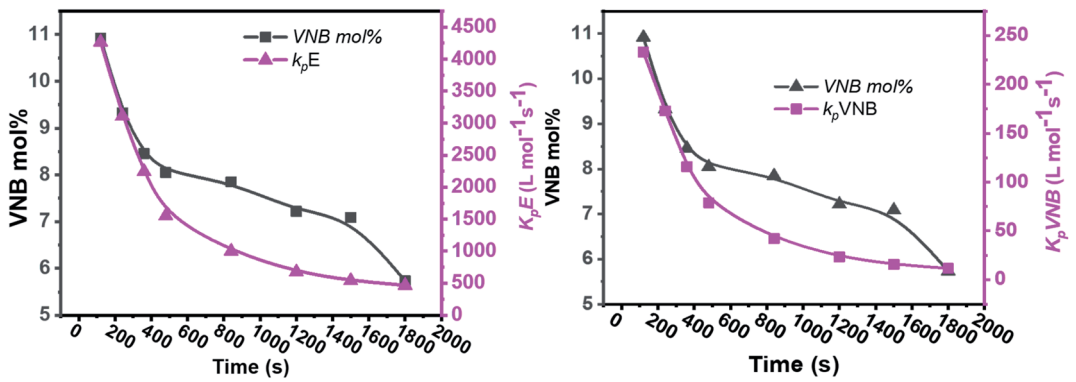

Fig. 5 Relationship between polymerization time and alteration in the propagation rate constants k_pE and k_pVNB and the mole% of VNB in the E/VNB copolymers.

ENB are less crystalline. Simultaneously, E/P and E/ENB are nearly amorphous, have low thermal values, and are comparatively easily dissolved in toluene. This difference may be due to the lower diffusion barrier in the E/VNB system and higher propagation rate content.

The diffusion barrier described the reasonable decay of k_pE and k_pVNB with t_p in the above discussion. However, the influence of [C*]/[Zr] on k_pE and k_pVNB must be considered. The [C*]/[Zr] fraction in the E/VNB copolymers is much lower than that in the polyethylene and E/ENB copolymers, particularly in the stable reaction stage. The [C*]/[Zr] generated in the later stage of the E/VNB copolymers has lower k_pE and k_pVNB values than k_pPE, k_pE, and k_pENB. It is well known that ENB, VNB, and P have a bulkier structure than the PE part of a polymeric catalyst such as metallocene in the shape of contact ion pairs, which may be unable to accept the coming VNB monomer for further coordination. Subsequently, it behaves as inactive or dormant sites and has a lower [C*]/[Zr] fraction. Consistent with earlier studies, the polymerization conditions employed in this study were the same. It is considered that the reaction parameters adopted in the given polymerizations are identical to that used in the previous work,[19,35,40,52] and thus it can be said that

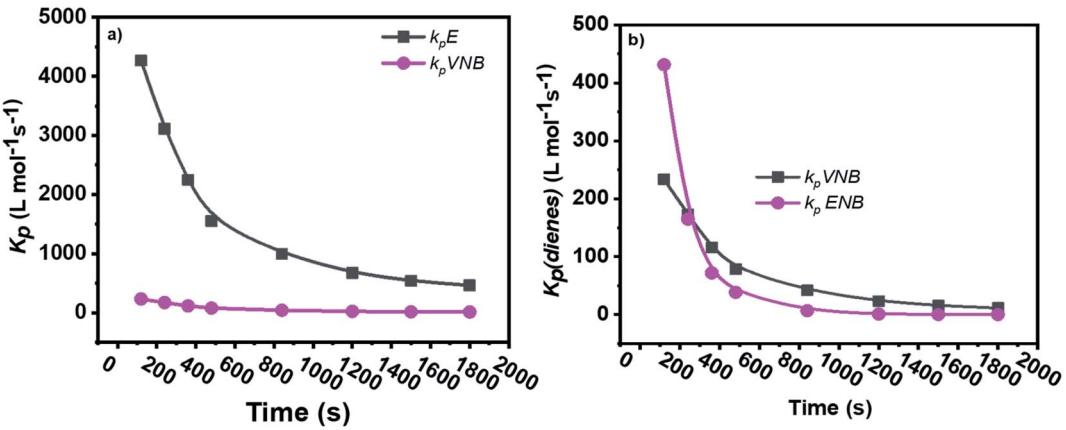

Fig. 6 Comparisons between the propagation rate constants of (a) k_pE and k_pVNB of E/VNB copolymers and (b) k_pVNB and k_pENB with the same reaction parameters.

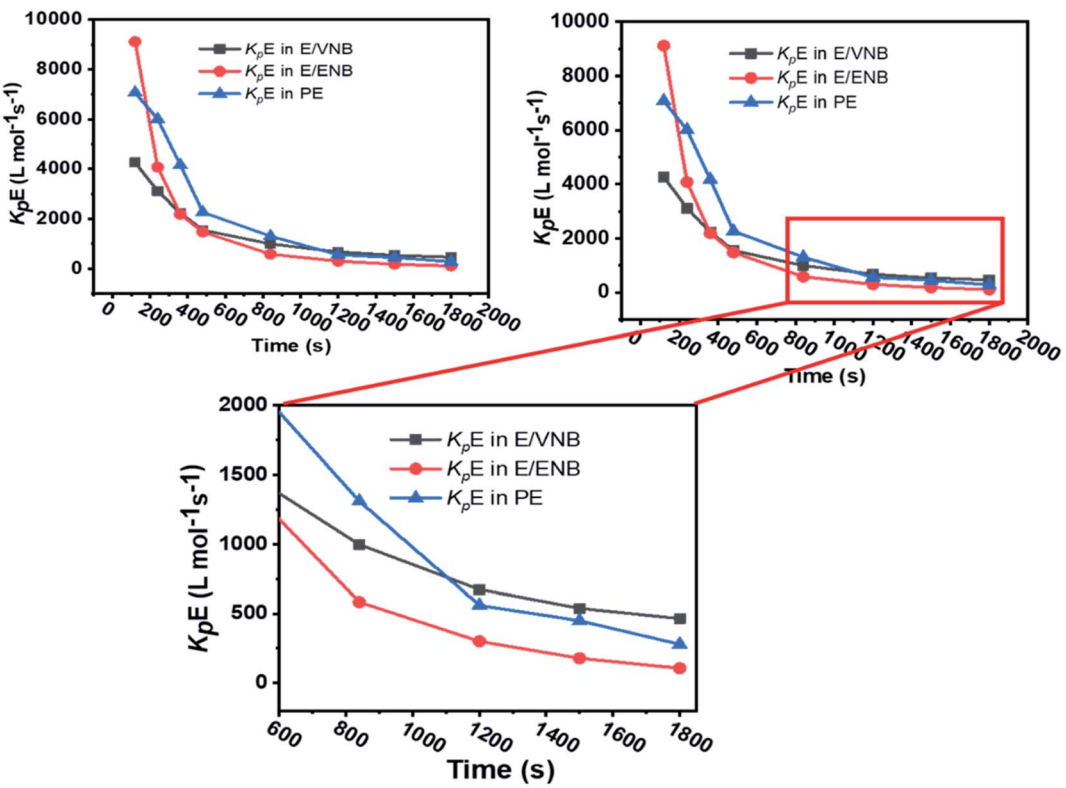

Fig. 7 Comparison of the propagation rate constants k_p of polyethylene (PE), E/ENB, and E/VNB polymerization.

changing the type of comonomers can influence the efficiency of the metallocene activation kinetic behaviors.

Discussion on mechanism

Our previous work investigated the kinetics of PE and PP.[19,36] The significate increase in M_w and MWD with reaction time was briefly explained through the earlier activation of the active centers with a longer cation–anion distance, and later with a shorter cation–anion distance.[17,19,53] The loose ion pairs found in the initial reaction time showed a higher polymerization rate, activity, and E/VNB yield with lower molecular weight. Subsequently, the interference from the counter-anion on the E and VNB monomers coordinated to the cationic active sites is poor and the conformational conversion of the propagation chain for β-hydrogen transfer becomes easier in the relatively open ion pair. According to Fan *et al.*, if the ion-pairs exhibit a shorter cation–anion distance, they will be less active for E coordination due to the strong interference from the counter anion for monomer coordination.[17,36] Given that we observed a similar increase in the M_w and $Đ$ of E/VNB with the reaction time, we can describe the phenomena with identical models, as shown in Scheme 1. The MWD curves of E/VNB were obtained at different reaction times (see ESI, Fig. S1†), which slowly increased with an increase in the reaction time t_p. The time-dependent change in the MWD for E/VNB was lower than that for PE. The time-dependent slow variations of MWD in t_p of 120–1800 s may be attributed to the slower increase in [C*]/[Zr] in the same period, and thus we can assume that the later-stage reaction activated active center has a longer cation distance than PE and produced E/VNB with a lower M_w.

The kinetic behaviors of the same catalyst for different monomers (PE, ENB, and VNB) can be described through this model. We compared the k_pE and k_pVNB with the k_pPE and k_pENB values in the first part of this paper, and we noticed that k_pE and k_pVNB were lower than k_pPE and k_pENB in most of the reaction times; meanwhile, the same catalyst system produced E/VNB with a lower M_w. This shows that the active site of the catalyst in the E/VNB copolymers has longer cation–anion distances than that for PE.

In the initial stage of E/VNB polymerization, the amount of active centers is slightly higher than that of PE, indicating that VNB sterically activated the active site in the metallocene precursor, which was dormant in the initial phase of PE. Despite the fact that the bicyclic VNB has an exocyclic and sterically endocyclic double bond, it is more difficult to synthesize than α-olefins such as propylene and 1-hexene. However, the lower [Zr]/[C*] fraction of the E/VNB copolymers than that of the PE and E/ENB copolymers at the stable and later stages can be attributed to the higher fraction of dormant sites in this system. This means that VNB as a comonomer deactivated the active sites in the same catalyst system, which was active in the PE and E/ENB polymerizations.

Scheme 2 shows the insertion of E into Zr–C and the insertion of VNB into Zr–E. VNB is sterically more interesting than P and 1-hexene, and the insertion barriers are more significant for Zr–C than P. The insertion of VNB as a comonomer in the system leads to a considerable decay inactivity. The steric impact of VNB, insertion in Zr–E, β-hydrogen transfer, repulsion between the catalyst ligand and VNB are explained by the mechanism presented in Scheme 2.

In the proposed mechanism (Scheme 2), the active catalytic sites $L_2Zr–CH_2–CH_2–VNB$ bearing propagation chain (A) possibly undergo β-H transfer reaction, and subsequently generate species (B) with a metal–hydrogen bond in the formation of $L_2Zr–H$, which is further converted into $L_2Zr–CH_2H_3$ (C) by inserting E into the $L_2Zr–H$ bond between the center of Zr and methyl hydrogen-produced $Zr–CH_2CH_3$ (D) species, which makes them unapproachable to the incoming VNB monomers. These species are involved in reducing the activity of the system. Many reports have been published in the literature on reactivating this type of dormant or inactive species. For example, Y. V. Kissin and colleagues investigated the co-co-monomer activation mechanism in heterogeneous Z–N catalyst systems through their model. They explained the E/P copolymerization catalyzed with Z–N and showed how

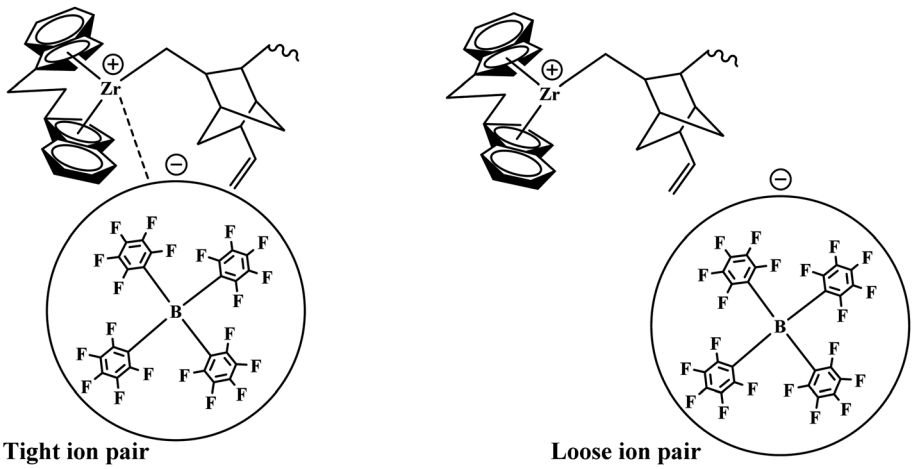

Scheme 1 Zirconocene/borate catalyst active centers with varying cation and anion distances.

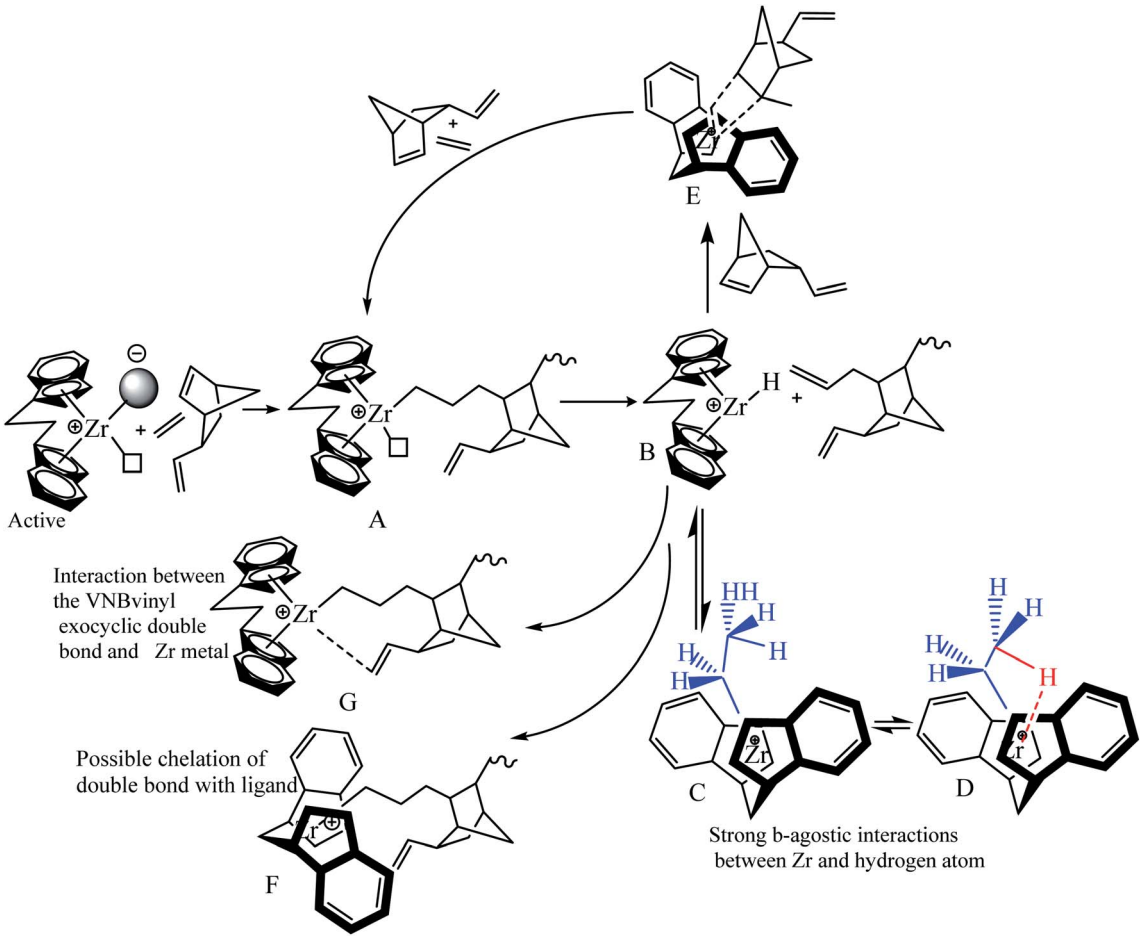

Scheme 2 Mechanistic model for the E/VNB copolymerization reactions, explaining how the inactive sites are formed by the steric impact of VNB, β-hydrogen transfer, and repulsion between the catalyst ligand VNB exocyclic π bonds, and how VNB reactivate them.

propylene activates the dormant ethylene sites. Similarly, Fan *et al.* employed this model in E/P copolymerization catalyzed with metallocene/MMAO and metallocene/TIBA/borate, and they analyzed that the insertion of the P comonomers in the zirconium–hydrogen bond (Zr–H) can bypass the reaction and significantly increase [Zr]/[C*], which was higher than that of their homopolymers. However, in the case of E/VMB polymerization, the insertion of the VNB zirconium–hydrogen bond (Zr–H) is very slow compared to ENB and P and hardly bypasses the reaction and converts to (E), leading to a slight increase in [Zr]/[C*], which is slightly higher than that for the homopolymerization of E. In addition, ENB and VNB are the nearly same family of olefins, but there are more robust β-agnostic contacts between the Zr metal and methyl hydrogen in VNB compared to ENB, resulting in a higher content of these dormant or inactive sites in the E/VNB copolymerization. This is the main reason for the lower [Zr]/[C*] fraction in the earlier and later stages than that previously reported for E/ENB copolymerization.

VNB polymerizes as cyclic diolefins with an alkyl substituent using an endocyclic π (–CH=CH–) bond and has a significant ring strain. The endocyclic π bond insertion of VNB in H–Zr increases the reaction rate and active centers through (E). This reaction, as mentioned above, was elucidated by the presence of peaks of exocyclic bonds in the polymer backbone, which can be utilized for additional post-polymerization investigation. Furthermore, the formation of L_2Zr–H and L_2Zr–CH_2H_3 can be achieved *via* the suitable adjustment of alkyl and zirconium due to the sufficient space between the L_2Zr^+–CH_2H_2–VNB cation and X^- anion. This prediction was supported by the significant reduction in the rate of VNB incorporation during the initial stages of the reaction. As illustrated in Table 2 and Fig. 2, 3, the active center fraction is 10–14% lower in the time of 120–480 s. With a further increase in the reaction time, it reached 33.7%, and the incorporation rate of VNB in the initial period was found to be higher than later. This indicates that the catalytic species L_2Zr^+–R.X.$^-$ activated initially can insert more VNB than the later activated catalytic species.

Conclusions

In this work, we investigated the kinetic behavior of ethylene/VNB copolymers catalyzed with *rac*-Et(Ind)$_2$ZrCl$_2$/TIBA/borate. The highest activity of 0.36×10^7 g mol_{Mt}^{-1} h^{-1} was achieved at 120 s, which decreased with a further increase in reaction time to 0.09×10^7 g mol_{Mt}^{-1} h^{-1}, and [Zr]/[*C] considerably increased, and consequently tended to the stable level of

31.67%. The E/VNB copolymers containing higher than 5 mol% VNB were soluble in 1,2,4-trichlorobenzene at 120 °C. The MWD was broader and significantly greater than 2, indicating the presence of multiple active sites in the system. The molecular weight decreased in the initial polymerization time and slightly increased with an increase in the reaction time. The crystalline (ΔH_m) temperature varied from 9 to 16 (J g^{-1}) and melting temperature (T_m) ranged from 100 °C to 120 °C. The crystallinity of the E/VNB copolymer was lower and its initial polymerization rates (R_pE and R_pVNB) were higher due to the more significant insertion of VNB in the growing polymer chain. The propagation rate constants k_pE and k_pVNB were much higher at the initial level (4266 and 233 L mol^{-1} s^{-1}) than later with values of 465 and 11.53 L mol^{-1} s^{-1}, respectively, which indicate that the minor diffusion barriers in the early stages are close to the actual propagation rate constant. The continual decrease in k_pE, and k_pVNB with t_p may be partially attributed to the reduction in the local-monomer concentration around the active site. In addition, the lower k_pE and k_pVNB in the later stage compared to earlier could be due to the lower mol% of VNB, which reduced the amorphous properties and hardly liquefied in the reaction solvent, subsequently leading to a higher diffusion barrier in the later system. The lower [C*]/[Zr] ratio of the E/VNB copolymers in both the early and stable stages and poor amorphous properties with lower VNB mol% at a later stage require the use of a specific kinetic mechanism that assumes the low activity of developing polymer chains containing one of $ZrCH_2CH_3$-type dormant site by β-agostic contact between the methyl hydrogens and the cationic Zr center and the interaction between the Zr metal and VNB endocyclic π bonds.

Conflicts of interest

The representative authors have no conflict of interest to disclose in any capacity, either competing or financial.

Acknowledgements

The authors are thankful to the National Natural Foundation of China (51803081) for their financial support.

References

1 D. L. Nelsen, B. J. Anding, J. L. Sawicki, M. D. Christianson, D. J. Arriola and C. R. Landis, Chromophore quench-labeling: an approach to quantifying catalyst speciation as demonstrated for (EBI)$ZrMe_2$/$B(C6F5)_3$-catalyzed polymerization of 1-hexene, *ACS Catal.*, 2016, **6**(11), 7398–7408.

2 A. Shamiri, M. H. Chakrabarti, S. Jahan, M. A. Hussain, W. Kaminsky, P. V. Aravind and W. A. Yehye, The influence of Ziegler-Natta and metallocene catalysts on polyolefin structure, properties, and processing ability, *Materials*, 2014, **7**(7), 5069–5108.

3 W. Kaminsky and M. Arndt, Metallocenes for polymer catalysis, in *Polymer Synthesis/Polymer Catalysis*, Springer, 1997, pp. 143–187.

4 W. Kaminsky, Highly active metallocene catalysts for olefin polymerization, *J. Chem. Soc., Dalton Trans.*, 1998, (9), 1413–1418.

5 P. S. Kulyabin, G. P. Goryunov, M. I. Sharikov, V. V. Izmer, A. Vittoria, P. H. Budzelaar, V. Busico, A. Z. Voskoboynikov, C. Ehm and R. Cipullo, ansa-Zirconocene Catalysts for Isotactic-Selective Propene Polymerization at High Temperature: A Long Story Finds a Happy Ending, *J. Am. Chem. Soc.*, 2021, **143**(20), 7641–7647.

6 A. Ali, A. Naveed, T. Rasheed, T. Aziz, M. Imran, Z.-K. Zhang, M. W. Ullah, A. A. Kubar, A. U. Rehman and Z. Fan, Methods for Predicting Ethylene/Cyclic Olefin Copolymerization Rates Promoted by Single-Site Metallocene: Kinetics Is the Key, *Polymers*, 2022, **14**(3), 459.

7 K. Angermund, G. Fink, V. R. Jensen and R. Kleinschmidt, Toward quantitative prediction of stereospecificity of metallocene-based catalysts for α-olefin polymerization, *Chem. Rev.*, 2000, **100**(4), 1457–1470.

8 V. Busico, L. Caporaso, R. Cipullo, L. Landriani, G. Angelini, A. Margonelli and A. Segre, Propene Polymerization Promoted by C_2-Symmetric Metallocene Catalysts: From Atactic to Isotactic Polypropene in Consequence of an Isotope Effect, *J. Am. Chem. Soc.*, 1996, **118**(8), 2105–2106.

9 M. D. Bruce, G. W. Coates, E. Hauptman, R. M. Waymouth and J. W. Ziller, Effect of metal on the stereospecificity of 2-arylindene catalysts for elastomeric polypropylene, *J. Am. Chem. Soc.*, 1997, **119**(46), 11174–11182.

10 E. S. Cueny, H. C. Johnson, B. J. Anding and C. R. Landis, Mechanistic studies of hafnium-pyridyl amido-catalyzed 1-octene polymerization and chain transfer using quench-labeling methods, *J. Am. Chem. Soc.*, 2017, **139**(34), 11903–11912.

11 A. C. Brezny and C. R. Landis, Recent developments in the scope, practicality, and mechanistic understanding of enantioselective hydroformylation, *Acc. Chem. Res.*, 2018, **51**(9), 2344–2354.

12 M. A. Naseer, M. K. Tufail, A. Ali, S. Hussain, U. Khan and H.-B. Jin, Review on Computational-Assisted to Experimental Synthesis, Interfacial Perspectives of Garnet-Solid Electrolytes for All-Solid-State Lithium Batteries, *J. Electrochem. Soc.*, 2021, **168**, 060529.

13 A. Ali, T. Aziz, J. Zheng, F. Hong, M. F. Awad, S. Manan, F. Haq, A. Ullah, M. N. Shah, Q. Javed, A. A. Kubar and L. Guo, Modification of Cellulose Nanocrystals with 2-Carboxyethyl Acrylate in the Presence of Epoxy Resin for Enhancing Its Adhesive Properties, *Front. Bioeng. Biotechnol.*, 2022, **9**, 797672.

14 R. Leino, F. J. Gómez, A. P. Cole and R. M. Waymouth, Syndiospecific Propylene Polymerization with C_1 Symmetric Group 4 ansa-Metallocene Catalysts, *Macromolecules*, 2001, **34**(7), 2072–2082.

15 J. Huang and G. L. Rempel, Kinetic study of propylene polymerization using Et$(H_4Ind)_2ZrCl_2$/methylalumoxane catalysts, *Ind. Eng. Chem. Res.*, 1997, **36**(4), 1151–1157.

16 A. Vittoria, V. Busico, F. D. Cannavacciuolo and R. Cipullo, Molecular kinetic study of "chain shuttling" olefin copolymerization, *ACS Catal.*, 2018, **8**(6), 5051–5061.

17 A. Ali, N. Muhammad, S. Hussain, M. I. Jamil, A. Uddin, T. Aziz, M. K. Tufail, Y. Guo, T. Wei and G. Rasool, Kinetic and thermal study of ethylene and propylene homo polymerization catalyzed by ansa-zirconocene activated with alkylaluminum/borate: effects of alkylaluminum on polymerization kinetics and polymer structure, *Polymers*, 2021, **13**(2), 268.

18 F. Song, R. D. Cannon and M. Bochmann, Zirconocene-catalyzed propene polymerization: a quenched-flow kinetic study, *J. Am. Chem. Soc.*, 2003, **125**(25), 7641–7653.

19 A. Ali, M. A. Akram, Y. Guo, H. Wu, W. Liu, A. Khan, X. Liu, Z. Fu and Z. Fan, Ethylene–propylene copolymerization and their terpolymerization with dienes using ansa-zirconocene catalysts activated by borate/alkylaluminum, *J. Macromol. Sci., Part A: Pure Appl.Chem.*, 2020, **57**(2), 156–164.

20 A. Ali, M. K. Tufail, M. I. Jamil, W. Yaseen, N. Iqbal, M. Hussain, A. Ali, T. Aziz, Z. Fan and L. Guo, Comparative Analysis of Ethylene/Diene Copolymerization and Ethylene/Propylene/Diene Terpolymerization Using Ansa-Zirconocene Catalyst with Alkylaluminum/Borate Activator: The Effect of Conjugated and Nonconjugated Dienes on Catalytic Behavior and Polymer Microstructure, *Molecules*, 2021, **26**(7), 2037.

21 C. R. Landis and M. D. Christianson, Metallocene-catalyzed alkene polymerization and the observation of Zr-allyls, *Proc. Natl. Acad. Sci. U. S. A.*, 2006, **103**(42), 15349–15354.

22 Z. Liu, E. Somsook and C. R. Landis, A 2H-labeling scheme for active-site counts in metallocene-catalyzed alkene polymerization, *J. Am. Chem. Soc.*, 2001, **123**(12), 2915–2916.

23 C. R. Landis, D. R. Sillars and J. M. Batterton, Reactivity of secondary metallocene alkyls and the question of dormant sites in catalytic alkene polymerization, *J. Am. Chem. Soc.*, 2004, **126**(29), 8890–8891.

24 E. S. Cueny, H. C. Johnson and C. R. Landis, Selective quench-labeling of the hafnium-pyridyl amido-catalyzed polymerization of 1-octene in the presence of trialkyl-aluminum chain-transfer reagents, *ACS Catal.*, 2018, **8**(12), 11605–11614.

25 H. C. Johnson, E. S. Cueny and C. R. Landis, Chain transfer with dialkyl zinc during hafnium–pyridyl amido-catalyzed polymerization of 1-octene: relative rates, reversibility, and kinetic models, *ACS Catal.*, 2018, **8**(5), 4178–4188.

26 M. F. Ryan, A. R. Siedle, M. J. Burk and D. E. Richardson, Parameter scale for substituent effects in cyclopentadienyl complexes based on gas-phase electron-transfer equilibrium studies of ruthenocene derivatives, *Organometallics*, 1992, **11**(12), 4231–4237.

27 A. Siedle, W. Lamanna, R. Newmark, J. Stevens, D. Richardson and M. Ryan, The role of non-coordinating anions in homogeneous olefin polymerization, in *Makromolekulare Chemie Macromolecular Symposia*, Wiley Online Library, 1993, pp. 215–224.

28 B. M. Moscato, B. Zhu and C. R. Landis, Mechanistic investigations into the behavior of a labeled zirconocene polymerization catalyst, *Organometallics*, 2012, **31**(5), 2097–2107.

29 E. S. Cueny and C. R. Landis, The hafnium-pyridyl amido-catalyzed copolymerization of ethene and 1-octene: how small amounts of ethene impact catalysis, *ACS Catal.*, 2019, **9**(4), 3338–3348.

30 A. Uddin, R. Khatoon, D. Estevez, M. Salem, A. Ali, S. Attique, J. Lu and F. Qin, Waste Paper Cellulose Based-Mos2 Hybrid Polymer Composites: Towards Sustainable Green Shielding, Available at SSRN 4044245.

31 A. Naveed, A. Ali, T. Rasheed, X. Wang, P. Ye, X. Li, Y. Zhou, S. Mingru and Y. Liu, Revisiting recent and traditional strategies for surface protection of Zn metal anode, *J. Power Sources*, 2022, **525**, 231122.

32 E. S. Cueny, L. R. Sita and C. R. Landis, Quantitative validation of the living coordinative chain-transfer polymerization of 1-hexene using chromophore quench labeling, *Macromolecules*, 2020, **53**(14), 5816–5825.

33 J. C. Chien and W. M. Tsai, Zirconocenium cation catalysis of propene polymerization, in *Makromolekulare Chemie Macromolecular Symposia*, Hüthig & Wepf Verlag, Basel, 1993, vol. 66, pp. 141–156.

34 W. Yaseen, M. Xie, B. A. Yusuf, Y. Xu, N. Ullah, M. Rafiq, A. Ali and J. Xie, Synergistically coupling of Co/Mo_2C/$Co_6Mo_6C_2$@C electrocatalyst for overall water splitting: the role of carbon precursors in structural engineering and catalytic activity, *Appl. Surf. Sci.*, 2022, **579**, 152148.

35 A. Ali, M. I. Jamil, A. Uddin, M. Hussain, T. Aziz, M. K. Tufail, Y. Guo, B. Jiang, Z. Fan and L. Guo, Kinetic and thermal study of ethylene-propylene copolymerization catalyzed by ansa-zirconocene activated with alkylaluminium/borate: effects of linear and branched alkylaluminium compounds as cocatalyst, *J. Polym. Res.*, 2021, **28**(5), 1–15.

36 Y. Guo, Z. Zhang, W. Guo, A. Khan, Z. Fu, J. Xu and Z. Fan, Kinetics and mechanism of metallocene-catalyzed olefin polymerization: comparison of ethylene, propylene homopolymerizations, and their copolymerization, *J. Polym. Sci., Part A: Polym. Chem.*, 2017, **55**(5), 867–875.

37 A. Khan, Y. Guo, Z. Zhang, A. Ali, Z. Fu and Z. Fan, Kinetics of short-duration ethylene–propylene copolymerization with $MgCl_2$-supported Ziegler–Natta catalyst: differentiation of active centers on the external and internal surfaces of the catalyst particles, *J. Appl. Polym. Sci.*, 2018, **135**(12), 46030.

38 M. A. Akram, X. Liu, B. Jiang, B. Zhang, A. Ali, Z. Fu and Z. Fan, Effect of alkylaluminum cocatalyst on ethylene/1-hexene copolymerization and active center distribution of $MgCl_2$-supported Ziegler-Natta catalyst, *J. Macromol. Sci., Part A: Pure Appl.Chem.*, 2021, 1–11.

39 A. Ali, M. Nadeem, J. Lu, J. M. Moradian, T. Rasheed, T. Aziz, C. Maouche, Y. Guo, M. Awais and F. Zhiqiang, Rapid kinetic evaluation of homogeneous single-site metallocene catalysts and cyclic diene: how do the catalytic activity, molecular weight, and diene incorporation rate of olefins affect each other?, *RSC Adv.*, 2021, **11**(50), 31817–31826.

40 B. Jiang, B. Zhang, Y. Guo, A. Ali, W. Guo, Z. Fu and Z. Fan, Effects of titanium dispersion state on distribution and reactivity of active centers in propylene polymerization with $MgCl_2$-supported Ziegler-Natta catalysts: a kinetic

study based on active center counting, *ChemCatChem*, 2020, **12**(20), 5140–5148.

41 R. Fang, J. Pi, T. Wei, A. Ali and L. Guo, Stimulus-Responsive Polymers Based on Polypeptoid Skeletons, *Polymers*, 2021, **13**(13), 2089.

42 B. Jiang, B. Zhang, Y. Guo, A. Ali, W. Guo, Z. Fu and Z. Fan, Effects of titanium dispersion state on distribution and reactivity of active centers in propylene polymerization with $MgCl_2$-supported Ziegler-Natta catalysts: a kinetic study based on active center counting, *ChemCatChem*, 2020, **12**(20), 5140–5148.

43 S. I. Chowdhury, R. Tanaka, Y. Nakayama and T. Shiono, Copolymerization of norbornene and conjugated dienes using anilinonaphthoquinone-ligated nickel complexes, *Polymer*, 2020, **187**, 122094.

44 S.-S. Choi and Y.-K. Kim, Analysis of 5-ethylidene-2-norbornene in ethylene-propylene-diene terpolymer using pyrolysis-GC/MS, *Polym. Test.*, 2011, **30**(5), 509–514.

45 S. Ahmadjo, H. Arabi, M. Nekoomanesh, G. H. Zohuri, M. M. Mortazavi and G. Naderi, Terpolymerization of Ethylene/Propylene/Diene Monomers Using $(2\text{-PhInd})_2ZrCl_2$ Metallocene Catalysts, *Macromol. React. Eng.*, 2010, **4**(11–12), 707–714.

46 M. I. Jamil, Q. Wang, A. Ali, M. Hussain, T. Aziz, X. Zhan and Q. Zhang, Slippery Photothermal Trap for Outstanding Deicing Surfaces, *Journal of Bionic Engineering*, 2021, **18**(3), 548–558.

47 G. Rasool, A. Shafiq, Y.-M. Chu, M. S. Bhutta and A. Ali, Optimal Homotopic Exploration of Features of Cattaneo-Christov Model in Second Grade Nanofluid Flow via Darcy-Forchheimer Medium Subject to Viscous Dissipation and Thermal Radiation, *Comb. Chem. High Throughput Screening*, 2021, 34477515.

48 B. Jongsomjit, S. Phoowakeereewiwat, S. Thongyai, T. Shiono and P. Praserthdam, Impact of diene addition on properties for ethylene–propylene copolymerization with rac-Et $[Ind]_2ZrCl_2$/MAO catalyst, *Mater. Lett.*, 2005, **59**(28), 3771–3774.

49 A. Ali, A. Uddin, M. I. Jamil, X. Shen, M. Abbas, T. Aziz, M. Hussain, S. Hussain, R. Fang and Z. Fan, Kinetics and mechanistic investigations of ethylene-propylene copolymerizations catalyzed with symmetrical metallocene and activated by TIBA/borate, *J. Organomet. Chem.*, 2021, 121929.

50 S. Marathe and S. Sivaram, Regioselective copolymerization of 5-vinyl-2-norbornene with ethylene using zirconocene-methylaluminoxane catalysts: a facile route to functional polyolefins, *Macromolecules*, 1994, **27**(5), 1083–1086.

51 J. C. Randall, A review of high resolution liquid ^{13}carbon nuclear magnetic resonance characterizations of ethylene-based polymers, *J. Macromol. Sci., Rev. Macromol. Chem. Phys.*, 1989, **29**(2–3), 201–317.

52 A. Ali, M. Nadeem, J. Lu, J. M. Moradian, T. Rasheed, T. Aziz, C. Maouche, Y. Guo, M. Awais and F. Zhiqiang, Correction: rapid kinetic evaluation of homogeneous single-site metallocene catalysts and cyclic diene: how do the catalytic activity, molecular weight, and diene incorporation rate of olefins affect each other?, *RSC Adv.*, 2021, **11**(53), 33301.

53 A. Ali, X. Liu, Y. Guo, M. A. Akram, H. Wu, W. Liu, A. Khan, B. Jiang, Z. Fu and Z. Fan, Kinetics and mechanism of ethylene and propylene polymerizations catalyzed with ansa-zirconocene activated by borate/TIBA, *J. Organomet. Chem.*, 2020, **922**, 121366.